

## CLOSED FORM SOLUTION FOR FAILURE PRESSURE IN BEND-FREE PRESSURE VESSELS

S. Daghighi<sup>1\*</sup> and P. M. Weaver<sup>2</sup>

<sup>1</sup> Bernal Institute, University of Limerick, Postdoctoral Researcher, Limerick, Ireland

<sup>2</sup> Bernal Institute, University of Limerick, Professor and Bernal Chair, Limerick, Ireland

\* Corresponding author (Shahrzad.Daghighi@ul.ie)

**Keywords:** Pressure Vessels, Composite Structures, Stiffness Tailoring, Failure Performance

### ABSTRACT

Pressure vessels are widely used in many industries to store and transport liquids and gases. Among the growing body of research in the design of pressure vessels, a new bend-free concept has been devised that uses the benefits of composite materials to tailor the stiffness spatially through the structure using the variable angle tow (VAT) technique. Failure is an important factor in designing pressure vessels that should be predicted accurately in order to ensure a safe design. Previous failure analysis revealed excellent performance for the bend-free VAT design pressure vessel in comparison with isotropic and constant stiffness composite pressure vessels made of straight fibre trajectories. The feasible bend-free design space is sufficiently large to address other considerations while tailoring the stiffness of structures. However, research to date has not considered the failure load as a design parameter in the bend-free design methodology. In this study, a general analytical expression representing the failure pressure that is valid for all locations in the bend-free vessel is developed. This expression can be used to control the performance of the bend-free pressure vessel while tailoring the stiffness analytically without the need for further numerical analysis. Therefore, it is possible to select the fibre tow trajectory within the bend-free design space for each location in the structure, which has the best failure performance compared to other fibre tow trajectories that result in the bend-free state in structures.

### 1 INTRODUCTION

Recently, there has been growing interest in hydrogen as an energy source all over the world. One of the main reasons for this interest is that using hydrogen as an energy source does not emit carbon dioxide, which makes it a potential solution for reaching a zero-carbon economy. Another advantage of hydrogen is its storage potential, making it possible to store renewable energy in large quantities and for a long period of time. As such, it provides an excellent opportunity to have a flexible energy system in which supply and demand can be balanced. However, hydrogen has a low energy per volume, indicating the need for pressure vessels that can withstand high internal pressures [1]. Therefore, using hydrogen as a power source is leading to increasing interest in designing efficient infrastructure, such as pressurised vessels or gas grids, for the storage and transportation of hydrogen.

The ratio between the volume of the pressure vessel for storing media and the volume of the circumscribed rectangular prism, which represents the space occupied by the pressure vessel, is defined as packing efficiency. For pressure vessels and storage purposes, packing efficiency is an important factor. Pressure vessels with larger packing efficiencies enable storing more media in the same amount of space. An appealing solution for achieving good packing efficiency is represented by non-circular pressure vessels. However, one of the difficulties arising from non-circular pressure vessels is the bending stress that inevitably arises in conventional designs caused by internal pressure [2]. The bending stress elevates stress levels beyond that of similar circular pressure vessels and, as a consequence, is countered by making it thicker, making the design inefficient due to the weight increase [3]. Alternatively, composite materials can be used to benefit from tailoring the stiffness spatially throughout the structure in order to suppress the bending stresses, which can result in a bend-free design [4-8]. Bend-free pressure vessels that can be obtained by variable stiffness composite designs can redistribute the in-plane stress gradient through the thickness to be more uniform which results in increasing the

overall load-carrying capacity and significant weight reduction. These advantages make bend-free composite vessels potential candidates for the next generation of pressure vessels that can also be considered as a solution for challenges in hydrogen storage.

Failure load plays an important role in designing pressure vessels, and it should be predicted accurately to assure a safe design. Previous failure analysis revealed an approximately 200% failure performance improvement for the bend-free VAT design pressure vessel compared to isotropic and constant stiffness composite pressure vessels with straight fibre tow trajectories [9, 10]. However, the failure load has not been considered as a design parameter to date in bend-free design methodology. The feasible design region for the current bend-free design concept is sufficiently large to be capable of considering other design parameters, such as failure load in the methodology. In other words, a design concept that tailors the stiffness throughout the vessel for obtaining the bend-free pressure vessel with the highest possible failure load within the bend-free design domain can be developed.

To this end, in Section 2, a failure envelope in lamination parameter design space proposed by IJsselmuiden et al. [11] is considered for super ellipsoids of revolution under internal pressure. This expression is simplified by imposing the bend-free conditions, which resulted in a closed-form solution for failure pressure in bend-free super ellipsoids of revolution. This expression is then used in Section 3 to assess the failure performance of the structure for each fibre tow trajectory that results in the bend-free state. Finally, in Section 4, the proposed design is verified numerically using finite element analysis in ABAQUS.

## 2 ANALYTICAL EXPRESSION FOR FAILURE PRESSURE IN THE BEND-FREE DESIGN

In this section, an analytical expression representing the maximum failure pressure of bend-free super ellipsoids of revolution is developed. The geometry of super ellipsoids of revolution is expressed by

$$\left[ \left( \frac{X}{a} \right)^2 + \left( \frac{Y}{a} \right)^2 \right]^{\frac{N}{2}} + \left( \frac{Z}{b} \right)^N = 1, \quad (1)$$

where  $a$  and  $b$  are two semi-axes, and  $N$  is the shape parameter, which controls the degree of sharpness at corners in any plane passing through the axis of revolution ( $Z$  axis), i.e.  $X$ - $Z$  and  $Y$ - $Z$  plane, in the super ellipsoids of revolution, as shown in Fig. 1 [12]. It is worth noting that  $N=2$  represents a special case of an ellipsoid of revolution, and the cross-section in any plane passing through the axis of revolution tends to rectangular shapes for larger values of  $N$ .

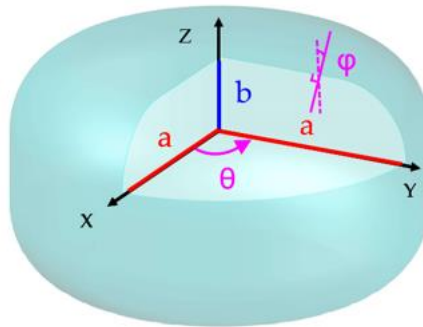


Fig. 1 Geometry of a super ellipsoid of revolution.

The bend-free design requires both bending moments and curvature changes to be simultaneously suppressed in the structure. Suppressing the bending moment results in moment-less states in the structure, while suppressing the curvature changes results in curvature-less states in the structure [4]. For super ellipsoids of revolution with moment-less states, in-plane stress resultants are [5, 13]

$$\begin{cases} N_\varphi = \frac{Pr_\theta}{2}, \\ N_\theta = N_\varphi(2 - \Delta), \\ N_{\varphi\theta} = 0, \end{cases} \quad (2)$$

where

$$\begin{aligned} \Delta = \frac{r_\theta}{r_\varphi} &= (N - 1) \cdot K^{\frac{-N}{N-1}} \cdot \cos \varphi^{\frac{N-2}{N-1}} \cdot \left[ \sin \varphi^{\frac{N}{N-1}} + (K \cos \varphi)^{\frac{N}{N-1}} \right], \\ r_\theta &= a \cdot (\sin \varphi)^{-1} \cdot \left[ 1 + (K \cot \varphi)^{\frac{N}{N-1}} \right]^{\frac{-1}{N}}, \\ K &= \frac{b}{a}. \end{aligned} \quad (3)$$

In this expression,  $P$  is the internal pressure, and  $K$  is the aspect ratio. The constitutive equation for a bend-free structure in which both bending moments and curvature changes are simultaneously suppressed ( $\mathbf{M} = \boldsymbol{\kappa} = 0$ ) are [14]

$$\begin{bmatrix} \mathbf{N} \end{bmatrix} = \begin{bmatrix} \mathbf{A} \end{bmatrix} \begin{bmatrix} \boldsymbol{\varepsilon} \end{bmatrix}, \quad (4)$$

Where  $\mathbf{N}$  and  $\boldsymbol{\varepsilon}$  are in-plane stress resultants and membrane strains, respectively. Moreover,  $\mathbf{A}$  is the in-plane stiffness matrix. The in-plane stiffness matrix can be substituted in terms of lamination parameters ( $V_i^A$ ) and material invariants ( $U_i$ ). Therefore, Eq. 4 becomes

$$\begin{bmatrix} N_\varphi \\ N_\theta \end{bmatrix} = t \begin{bmatrix} U_1 + V_1^A U_2 + V_2^A U_3 & U_4 - V_2^A U_3 \\ U_4 - V_2^A U_3 & U_1 - V_1^A U_2 + V_2^A U_3 \end{bmatrix} \begin{bmatrix} \varepsilon_\varphi \\ \varepsilon_\theta \end{bmatrix}. \quad (5)$$

Considering the moment-less state, the geometry of super ellipsoids of revolution can be related to strains by [13]

$$\frac{r_\theta}{r_\varphi} = \frac{\varepsilon_\varphi}{\varepsilon_\theta}, \quad (6)$$

where  $r_\varphi$  and  $r_\theta$  are two geometrical radii of curvature and  $\varepsilon_\varphi$  and  $\varepsilon_\theta$  are strains in  $\varphi$  and  $\theta$  directions, respectively. As expressed in Eq. 2,  $\Delta = r_\theta/r_\varphi$ , therefore, from Eq. 6

$$\varepsilon_\varphi = \Delta \cdot \varepsilon_\theta. \quad (7)$$

$N_\varphi$  can be expressed in terms of  $\varepsilon_\theta$  by substituting for  $\varepsilon_\varphi$  from Eq. 7 in Eq. 5 as

$$N_\varphi = \left[ (U_1 + V_1^A U_2 + V_2^A U_3) \Delta + U_4 - V_2^A U_3 \right] \cdot \varepsilon_\theta. \quad (8)$$

Substituting for  $N_\varphi$  from Eq. 8 in the equilibrium equations (Eq. 2) gives

$$\varepsilon_\theta = \frac{Pr_\theta}{2t (U_1 \Delta + U_4 + V_1^A U_2 \Delta + V_2^A U_3 \Delta - V_2^A U_3)}. \quad (9)$$

A conservative failure envelope independent of fibre orientation has been proposed by IJsselmuiden et al. [11]

$$4u_6^2 I_2^2 - 4u_6 u_1 I_2^2 + 4 \left(1 - u_2 I_1 - u_3 I_1^2\right) (u_1 - u_6) + (u_4 + u_5 I_1)^2 = 0, \quad (10)$$

$$u_1^2 I_2^4 - I_2^2 (u_4 + u_5 I_1)^2 - 2u_1 I_2^2 \left(1 - u_2 I_1 - u_3 I_1^2\right) + \left(1 - u_2 I_1 - u_3 I_1^2\right)^2 = 0. \quad (11)$$

Each expression represents a surface traced out by the failure criterion for all ply orientations. In these equations,  $I_1$  and  $I_2$  are the volumetric strain invariant and the maximum shear strain, respectively, given by

$$\begin{aligned} I_1 &= \epsilon_x + \epsilon_y, \\ I_2 &= \sqrt{\frac{\epsilon_x - \epsilon_y}{2} + \epsilon_{xy}^2}, \end{aligned} \quad (12)$$

and  $U_i$  with ( $i=1, 2, \dots, 6$ ) are

$$\begin{aligned} u_1 &= \frac{(Q_{11} - Q_{12})^2}{X_T X_C} + \frac{(Q_{12} - Q_{22})^2}{Y_T Y_C} + \frac{(Q_{11} - Q_{12})(Q_{22} - Q_{12})}{X_T^2}, \\ u_2 &= \frac{1}{2} \left[ \left( \frac{1}{X_T} - \frac{1}{X_C} \right) (Q_{11} + Q_{12}) + \left( \frac{1}{Y_T} - \frac{1}{Y_C} \right) (Q_{12} + Q_{22}) \right], \\ u_3 &= \frac{1}{4} \left[ \frac{(Q_{11} + Q_{12})^2}{X_T X_C} + \frac{(Q_{12} + Q_{22})^2}{Y_T Y_C} - \frac{(Q_{12} + Q_{22})(Q_{11} + Q_{12})}{X_T^2} \right], \\ u_4 &= \left( \frac{1}{X_T} - \frac{1}{X_C} \right) (Q_{11} - Q_{12}) + \left( \frac{1}{Y_T} - \frac{1}{Y_C} \right) (Q_{12} - Q_{22}), \\ u_5 &= \frac{Q_{11}^2 - Q_{12}^2}{X_T X_C} + \frac{Q_{12}(Q_{22} - Q_{11})}{X_T^2} + \frac{Q_{12}^2 - Q_{22}^2}{Y_T Y_C}, \\ u_6 &= \frac{4Q_{66}^2}{S_L^2}, \end{aligned} \quad (13)$$

where  $X_T$ ,  $X_C$ ,  $Y_T$ ,  $Y_C$  and  $S_L$  are material strength properties as described in Table 1 and  $Q_{ij}$  are components of the reduced stiffness matrix given by

$$\begin{aligned} Q_{11} &= \frac{E_1}{1 - \nu_{12}\nu_{21}}, \\ Q_{12} &= \frac{\nu_{12}E_2}{1 - \nu_{12}\nu_{21}}, \\ Q_{22} &= \frac{E_2}{1 - \nu_{12}\nu_{21}}, \\ Q_{66} &= G_{12}. \end{aligned} \quad (14)$$

In this expression,  $E_1$ ,  $E_2$  and  $G_{12}$  are the longitudinal, transverse and in-plane shear moduli, respectively and  $\nu_{12}$  is the Poisson's ratio for a unidirectional lamina [15].

	Property	Value (MPa)
$X_T$	longitudinal tensile strength	2323.5
$X_C$	longitudinal compressive strength	-1017.5
$Y_T$	transverse tensile strength	62.3
$Y_C$	transverse compressive strength	-253.7
$S_L$	in-plane strength	89.6

Table 1: Material properties for IM7/8552 carbon-epoxy.

Eqs. 10 and 11 are second- and fourth-order expressions with respect to strains, respectively, and are independent of stacking sequence. As explained in [11], failure envelopes represented by Eqs. 10 and 11 do not intersect. However, they may become tangential to each other. The material properties determine whether the inner envelope is represented by the second-order (Eq. 10) or the fourth-order (Eq. 11) expression. In order to avoid failure, the inner envelope should be considered.

Bend-free super ellipsoids of revolution under uniform internal pressure are axisymmetric structures and shear-free ( $N_{\varphi\theta} = \varepsilon_{\varphi\theta} = 0$ ), which eliminates  $\varepsilon_{xy}$  from Eq. 12. Moreover, for bend-free structures,  $\varepsilon_{\varphi}$  and  $\varepsilon_{\theta}$  are related, as shown in Eq. 7 and for bend-free structures, only membrane strains exist, which allows Eq. 12 to simplify to

$$\begin{aligned} I_1 &= \varepsilon_{\theta}(\Delta + 1), \\ I_2 &= \sqrt{\left(\frac{\varepsilon_{\theta}(\Delta - 1)}{2}\right)^2}. \end{aligned} \quad (15)$$

Substituting for  $\varepsilon_{\theta}$  from Eq. 9 in Eq. 15 gives

$$\begin{aligned} I_1 &= \frac{Pr_{\theta}(\Delta + 1)}{2t(U_1\Delta + U_4 + V_1^A U_2\Delta + V_2^A U_3\Delta - V_2^A U_3)}, \\ I_2 &= \sqrt{\left(\frac{Pr_{\theta}(\Delta - 1)}{4t(U_1\Delta + U_4 + V_1^A U_2\Delta + V_2^A U_3\Delta - V_2^A U_3)}\right)^2}. \end{aligned} \quad (16)$$

The failure pressure at each location in the bend-free super ellipsoids of revolution can be obtained by substituting Eq. 16 in Eqs. 10 and 11 as

$$\begin{aligned} P^2 J_1 + P J_2 + J_3 &= 0, \\ P^4 J_4 + P^3 J_5 + P^2 J_6 + P J_7 + 1 &= 0, \end{aligned} \quad (17)$$

where  $J_1, J_2, J_3, J_4, J_5, J_6$  and  $J_7$  are

$$\begin{aligned}
J_1 &= \frac{r_\theta^2 \left[ (u_6^2 - u_1 u_6)(\Delta - 1)^2 + (4u_3 u_6 - 4u_1 u_3 + u_5^2)(\Delta + 1)^2 \right]}{4t^2 (U_1 \Delta + U_4 + V_1^A U_2 \Delta + V_2^A U_3 \Delta - V_2^A U_3)^2}, \\
J_2 &= \frac{r_\theta (\Delta + 1)(2u_6 u_2 - 2u_1 u_2 + u_4 u_5)}{t (U_1 \Delta + U_4 + V_1^A U_2 \Delta + V_2^A U_3 \Delta - V_2^A U_3)}, \\
J_3 &= u_4^2 + 4u_1 - 4u_6, \\
J_4 &= \frac{r_\theta^4 \left[ (u_1 + 4u_3)(\Delta - 1)^2 + 16u_3 \Delta \right]^2 - 4u_5^2 (\Delta^2 - 1)^2}{256t^4 (U_1 \Delta + U_4 + V_1^A U_2 \Delta + V_2^A U_3 \Delta - V_2^A U_3)^4}, \\
J_5 &= \frac{r_\theta^3 (\Delta + 1) \left[ (2u_1 u_2 + 4u_2 u_3 - u_4 u_5)(\Delta - 1)^2 + 16u_2 u_3 \Delta \right]}{16t^3 (U_1 \Delta + U_4 + V_1^A U_2 \Delta + V_2^A U_3 \Delta - V_2^A U_3)^3}, \\
J_6 &= \frac{r_\theta^2 \left[ 4u_2^2 (\Delta + 1)^2 - (2u_1 + 8u_3 + u_4^2)(\Delta - 1)^2 - 32u_3 \Delta \right]}{16t^2 (U_1 \Delta + U_4 + V_1^A U_2 \Delta + V_2^A U_3 \Delta - V_2^A U_3)^2}, \\
J_7 &= \frac{-r_\theta u_2 (\Delta + 1)}{t (U_1 \Delta + U_4 + V_1^A U_2 \Delta + V_2^A U_3 \Delta - V_2^A U_3)}.
\end{aligned} \tag{18}$$

For a known geometry and material properties, and by using Eq. 17, it is possible to find analytically the failure pressure at each location, represented by a known  $\varphi$ , in the bend-free super ellipsoids of revolution. It should be noted that Eqs. 17 are second-order and fourth-order equations and therefore have more than one solution. However, only the real and positive values for pressure are viable. The failure pressure is the minimum positive real value of pressure found from Eq. 17. In the next section, these expressions are used to obtain the failure pressure in a specific bend-free VAT super ellipsoid of revolution.

### 3 ANALYTICAL RESULTS FOR A VAT SUPER ELLIPSOID OF REVOLUTION

In this section, a specific super ellipsoid of revolution with  $N=2$ ,  $a=500$  mm,  $K=0.72$  with the material properties described in Table 2 is considered to be designed to have bend-free states under uniform internal pressure using the bend-free design methodology developed by Daghighi et al. [5]

Property	$E_{11}$	$E_{22}$	$E_{33}$	$G_{12}$	$G_{13}$	$G_{23}$	$\nu_{12}$	$\nu_{13}$	$\nu_{23}$
	GPa	GPa	GPa	GPa	GPa	GPa	-	-	-
Value	161	11.38	11.38	5.2	5.2	3.9	0.32	0.32	0.45

Table 2: Material properties for IM7/8552 carbon-epoxy [16].

The governing equation which dictates the bend-free state in super ellipsoids of revolution under uniform internal pressure is defined as [5]

$$-\Delta^2 + 2\Delta \left( \frac{U_1 - U_4 + U_2 V_1^A + 2U_3 V_2^A}{U_1 + U_2 V_1^A + U_3 V_2^A} \right) + \left( \frac{2U_4 - U_1 - 3U_3 V_2^A + U_2 V_1^A}{U_1 + U_2 V_1^A + U_3 V_2^A} \right) = 0. \quad (19)$$

In this expression,  $V_1^A$  and  $V_2^A$  are in-plane lamination parameters,  $U_i$  are material stiffness invariants, and  $\Delta$  is given by Eq. 3. The bend-free governing equation represented in Eq. 19 is used for stiffness tailoring. Therefore, considering a specific material system, for each location in the structure identified by a known  $\varphi$ , Eq. 19 gives a linear combination of  $V_1^A$  and  $V_2^A$  that results in a bend-free design. Lamination parameters are trigonometric functions of fibre orientation ( $\theta_1$ ) defined by [17]

$$\begin{pmatrix} V_1^A & V_2^A \end{pmatrix} = \frac{1}{2} \int_{-1}^1 (\cos 2\theta_1 \quad \cos 4\theta_1) d\bar{\xi}, \quad (20)$$

where  $\bar{\xi} = 2\frac{\xi}{t}$  is the normalised thickness, and they are not independent. For bend-free structures with balanced and symmetric laminates, the dependency of lamination parameters can be expressed by [18]

$$\left\{ \begin{array}{l} \text{Constraint 1: } 2(V_1^A)^2 - (V_2^A) - 1 \leq 0, \\ \text{Constraint 2: } |V_1^A| - 1 \leq 0, \\ \text{Constraint 3: } |V_2^A| - 1 \leq 0. \end{array} \right. \quad (21)$$

and it results in a convex two-dimensional feasible region, as shown in Fig. 2. For each location in the structure identified by a known  $\varphi$ , there are many combinations of  $V_1^A$  and  $V_2^A$ , represented by the red line in Fig. 2, within the feasible region that result in the bend-free design. Therefore, the bend-free design methodology is capable of including further design parameters. Failure pressure is an important design parameter in designing pressure vessels that can be included in this design methodology.

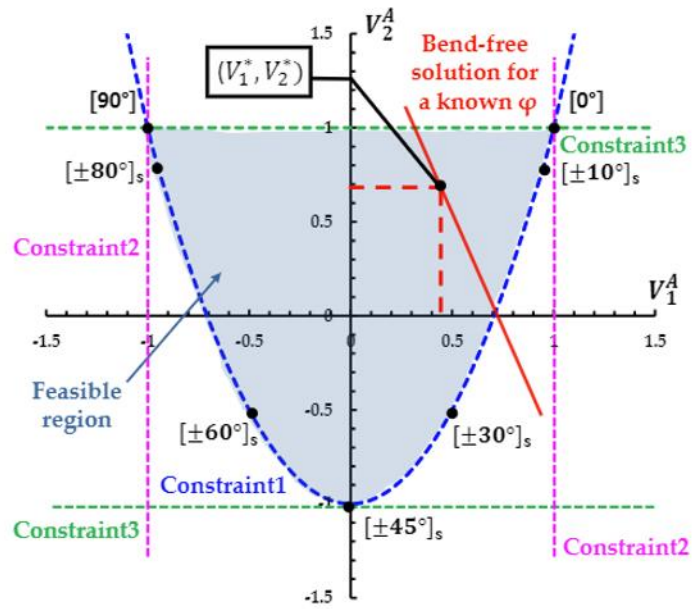


Fig. 2 Feasible region of bend-free state in  $V_1^A - V_2^A$  domain [8].

Eq. 17 can be used to assess the variation of failure pressure over the bend-free solution within the feasible region for each known  $\varphi$ . In this way, the combination of two lamination parameters ( $V_1^*$ ,  $V_2^*$ ) that provides the best failure performance among all possible combinations of ( $V_1^A$ ,  $V_2^A$ ) within the bend-free feasible region can be selected. In other words, the stiffness can be tailored throughout the structure to obtain a bend-free pressure vessel with the highest possible failure load.

Fig. 3 shows the 3D contour plots of the variation of the failure pressure for the bend-free solution within the feasible region for different locations (known  $\varphi$ ) over the super ellipsoid with  $N = 2$ ,  $a = 500$  mm,  $K = 0.72$  and the material properties described in Table 2. It should be noted that  $\varphi = 0^\circ$  refers to the pole while  $\varphi = 90^\circ$  refers to the equator.

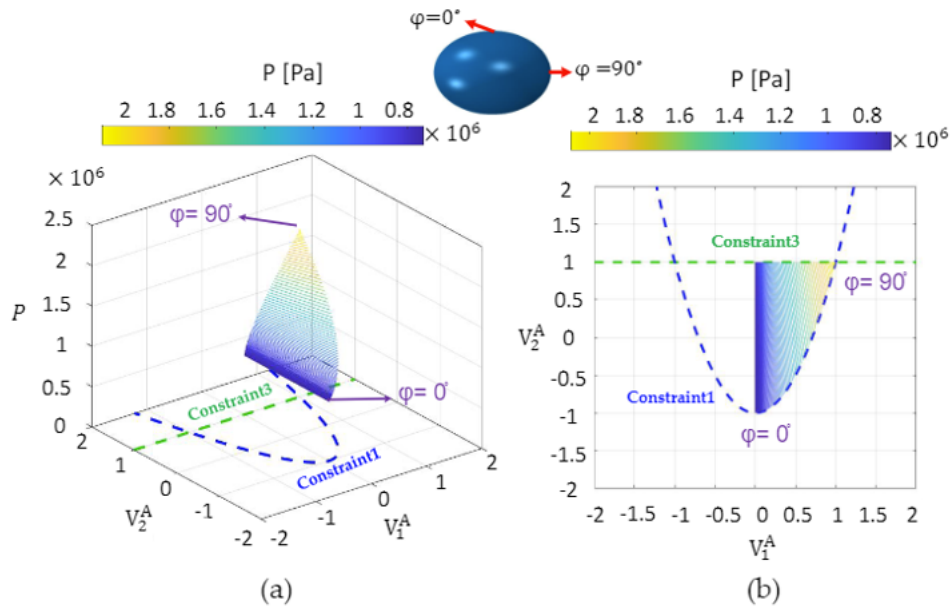


Fig. 3 3D contour plots of the variation of the failure pressure over the bend-free solution within the feasible region for different locations over the structure,  $\varphi$  changing from  $0^\circ$  to  $90^\circ$  in  $1^\circ$  steps. The structure is a super ellipsoid of revolution with  $N=2$ ,  $a=500$  mm and  $K=0.72$ .

As shown in Fig. 3, the pole has the smallest value of failure pressure compared to other locations and is, therefore, the critical area for failure in this structure. The variation of the failure pressure over the bend-free solution (given by Eq. 17) at  $\varphi = 65^\circ$  which is approximately located at one third of the distance from the equator to the pole, is shown in Fig. 4. For this example, the failure pressure increases when moving from the upper boundary (constraint3) to the lower boundary (constraint1) of the feasible region and reaches the maximum amount at the lower boundary. This finding indicates that the intersection of bend-free solution lines with the lower boundary of the feasible region gives the combination of  $(V_1^A, V_2^A)$  that results in a bend-free super ellipsoid of revolution with  $N=2$ ,  $a=500$  mm and  $K=0.72$ , which has the highest possible values for the failure load.

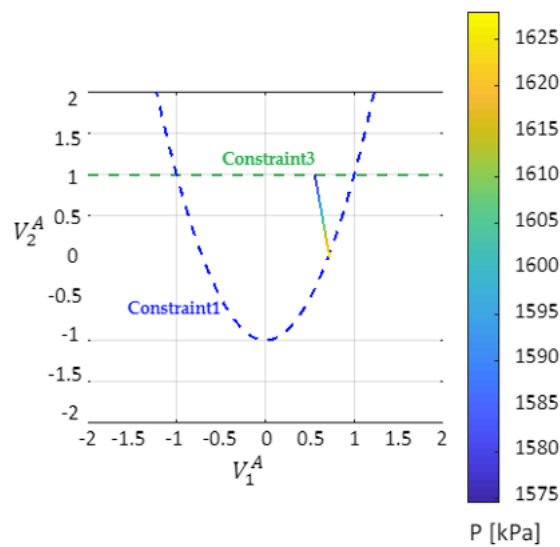


Fig. 4 The variation of the failure pressure over the bend-free solution at  $\varphi = 65^\circ$  for the case study of a super ellipsoid of revolution with  $N=2$ ,  $a=500$  mm and  $K=0.72$ .

#### 4 NUMERICAL VERIFICATION

In this section, the accuracy of the developed expression in Section 3 for predicting the failure pressure (Eq. 17) is verified numerically. Therefore, the stiffness of super ellipsoid of revolution described in Section 4 with  $N=2$ ,  $a=500$  mm,  $K=0.72$  and made of carbon epoxy IM7/8552 is tailored using the VAT technique, according to the analytical methodology described by Daghighi et al. [5], to have bend-free states. In order to have the best failure performance within the bend-free design using the VAT technique as concluded in Section 3, first, the intersection of solution lines with the lower boundary of the feasible region is used to extract tailored lamination parameters. Second, by considering a balanced symmetric laminate i.e.  $[\theta_1, -\theta_1]_s$ , the fibre tow trajectories corresponding to the tailored lamination parameters are found analytically using

$$\theta_1 = 0.5 \cdot \arccos(V_1^*) = 0.25 \cdot \arccos(V_2^*). \quad (22)$$

The fibre orientation distribution is plotted in Fig. 5 for the designed bend-free super ellipsoid of revolution. It should be noted that the fibre tow trajectory is the same for the locations with the same distance from the equator.

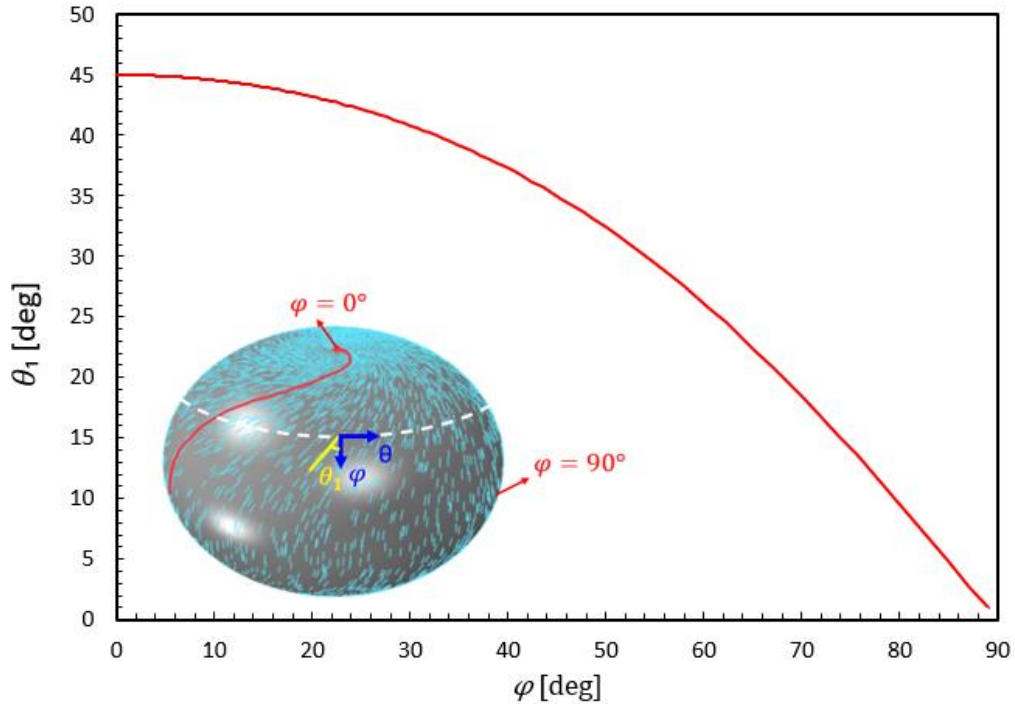


Fig. 5 Fibre orientation for the bend-free state in the super ellipsoid of revolution with  $N=2$ ,  $a=500$  mm and  $K=0.72$ , made of carbon epoxy IM7/8552.

This bend-free structure is modelled using S8R5 and STRI65 shell elements in ABAQUS. An in-house MATLAB code was used to associate the correct fibre tow trajectory, obtained from Eq. 22, to each finite element. Further details on the modelling can be found in [7]. The flowchart shown in Fig. 6 describes the approach taken in this study for obtaining the failure pressure numerically.

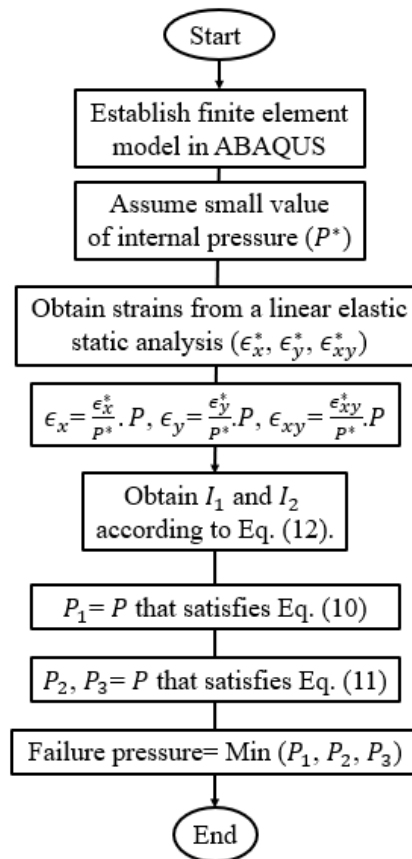


Fig. 6 Flowchart representing the finite element analysis.

The failure pressure at each location in the bend-free super ellipsoid of revolution is obtained analytically using Eq. 17. Fig. 7 compares the failure pressure at each location in the bend-free super ellipsoids of revolution that are found based on numerical and analytical approaches. As shown in Fig. 7, there is a good agreement between the numerical and analytical approaches with a maximum error of less than 0.31%, which confirms the accuracy of the analytical solution developed in this study.

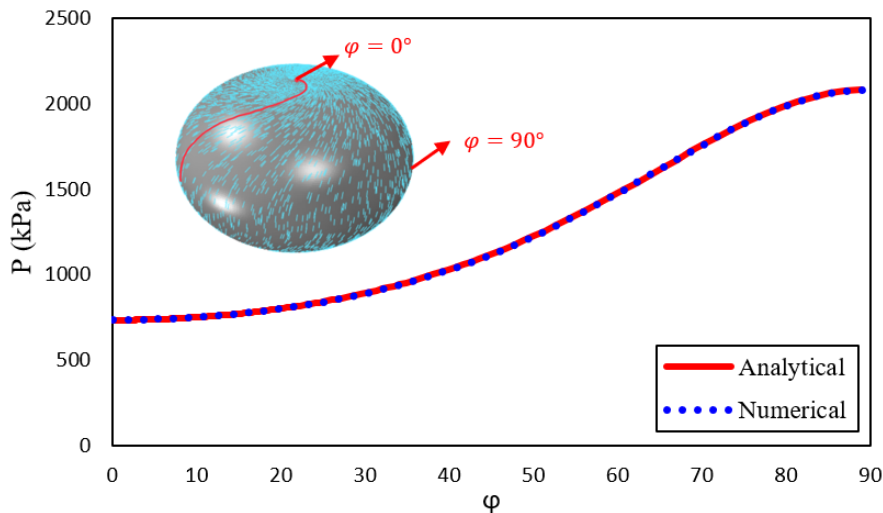


Fig. 7 Comparison of numerical and analytical failure pressure at each location in the bend-free VAT super ellipsoid of revolution with  $N=2$ ,  $\alpha=500$  mm and  $K=0.72$ , made of carbon epoxy IM7/8552

## 5 CONCLUSION

Failure pressure is an important design parameter for designing pressure vessels. Studying the failure performance of structures with complex geometries and stiffness properties usually requires expensive numerical studies. The current study aimed to develop a general analytical expression for failure pressure in the recently proposed bend-free VAT pressure vessels. The developed failure expression is written in a general form. Therefore, this expression can be used to predict the failure pressure analytically for a family of super ellipsoids of revolution with different geometries and material systems that are tailored using the VAT technique to have a bend-free state. This expression is then used in the bend-free design methodology to include the failure performance of the structure in the stiffness tailoring. The numerical results verified the accuracy of the failure pressure predicted by the proposed analytical expression with an error of less than 0.31%.

## ACKNOWLEDGEMENTS

The authors would like to thank Science Foundation Ireland (SFI) for funding Spatially and Temporally VARIABLE COMPOSITE Structures (VARICOMP) Grant No. (15/RP/2773) under its Research Professor programme.

## REFERENCES

- [1] U.S. Department of Energy, Hydrogen and Fuel Cell Technologies Office, "Hydrogen Storage," 2017. URL <https://www.energy.gov/eere/fuelcells/hydrogen-storage>.
- [2] Kolom, A. L., "Pressure vessel with a non-circular axial cross-section," Aug. 27 1991. US Patent 5,042,751.
- [3] Ray, S., and Das, G., "Chapter 17 - Process vessels," Process Equipment and Plant Design, edited by S. Ray and G. Das, Elsevier, 2020, pp. 629–666.
- [4] Daghighi, S., Rouhi, M., Zucco, G., and Weaver, P. M., "Bend-free design of ellipsoids of revolution using variable stiffness composites," Composite Structures, Vol. 233, 2020a, p. 111630.

- [5] Daghighi, S., Zucco, G., Rouhi, M., and Weaver, P. M., “Bend-free design of super ellipsoids of revolution composite pressure vessels,” *Composite Structures*, Vol. 245, 2020b, p. 112283.
- [6] Daghighi, S., “Structurally efficient composite super ellipsoidal shells,” PhD thesis, University of Limerick, Ireland, 2021. URL <https://hdl.handle.net/10344/10371>.
- [7] Daghighi, S., Zucco, G., and Weaver, P. M., “Design of Variable Stiffness Super Ellipsoidal Pressure Vessels under Thermo-mechanical Loading,” *AIAA SCITECH 2022 Forum*, 2022, p. 0869.
- [8] Daghighi, S., Zucco, G., and Weaver, P. M., “Design Methods for Variable-Stiffness Super-Ellipsoidal Pressure Vessels Under Thermomechanical Loading,” *AIAA Journal*, Vol. 0, No. 0, 0, pp. 1–14.
- [9] Daghighi, S., and Weaver, P. M., “Three-dimensional effects influencing failure in bend-free, variable stiffness composite pressure vessels,” *Composite Structures*, Vol. 262, 2021, p. 113346.
- [10] Daghighi, S., and Weaver, P. M., “Failure Performance of Bend-Free Variable Stiffness Composite Pressure Vessels,” *Proceedings of the American Society for Composites—Thirty-Sixth Technical Conference on Composite Materials*, 2021.
- [11] IJsselmuiden, S. T., Abdalla, M. M., and Gürdal, Z., “Implementation of strength-based failure criteria in the lamination parameter design space,” *AIAA journal*, Vol. 46, No. 7, 2008, pp. 1826–18348.
- [12] Barr, A. H., “Superquadrics and angle-preserving transformations,” *IEEE Computer graphics and Applications*, Vol. 1, No. 1, 1981, pp. 11–23.
- [13] Pao, Y., “Momentless Design of Composite Structures with Variable Elastic Constants,” *Journal of Composite Materials*, Vol. 3, No. 4, 1969, pp. 604–616.
- [14] White, S. C., and Weaver, P. M., “Bend-free shells under uniform pressure with variable-angle tow derived anisotropy,” *Composite Structures*, Vol. 94, No. 11, 2012, pp. 3207 – 3214.
- [15] Reddy, J. N., *Theory and analysis of elastic plates and shells*, CRC press, 2006.
- [16] Krueger, R., *Finite Element Analysis of Composite Joint Configurations with Gaps and Overlaps*, National Aeronautics and Space Administration, Langley Research Center, 2014.
- [17] Tsai, S. W., and Pagano, N. J., “Invariant properties of composite materials.” Tech. rep., Air force materials lab Wright-Patterson AFB Ohio, 1968.
- [18] Bloomfield, M. W., Diaconu, C., and Weaver, P., “On feasible regions of lamination parameters for lay-up optimisation of laminated composites,” *Proceedings of the Royal Society A: Mathematical, Physical and Engineering Sciences*, Vol. 465, No. 2104, 2009, pp. 1123–1143.